

Dual species matter qubit entangled with light

S.-Y. Lan, S. D. Jenkins, T. Chaneliere,[?] D. N. Matsukevich,^y

C. J. Campbell, R. Zhao, T. A. B. Kennedy, and A. Kuzmich
School of Physics, Georgia Institute of Technology, Atlanta, Georgia 30332-0430

(Dated: February 14, 2021)

We propose and demonstrate an atomic qubit based on a cold ^{85}Rb - ^{87}Rb isotopic mixture, entangled with a frequency-encoded optical qubit. The interface of an atomic qubit with a single spatial light mode, and the ability to independently address the two atomic qubit states, should provide the basic element of an interferometrically robust quantum network.

PACS numbers: 42.50.Dv, 03.65.Ud, 03.67.Mn

Quantum mechanics permits the secure communication of information between remote parties [1, 2, 3]. However, direct fiber based quantum communication over distances greater than about 100 km is challenging due to intrinsic fiber losses. To overcome this limitation it is necessary to take advantage of quantum state storage at intermediate locations on the transmission channel. Interconversion of the information from light to matter to light is therefore essential. It was the necessity to interface photonic communication channels and storage elements that lead to the proposal of the quantum repeater as an architecture for long-distance distribution of quantum information via qubits [4, 5].

Recently there has been rapid progress in interfacing photonic and stored atomic qubits. Two-ensemble encoding of matter qubits was used to achieve entanglement of photonic and atomic rubidium qubits and quantum state transfer from matter to light [6]. This was followed by a more robust single-ensemble qubit encoding [7], which led to full light-matter-light qubit interconversion and entanglement of two remote atomic qubits [8]. More recently, both two-ensemble and single-ensemble atomic qubits were reported using cesium gas [9, 10].

To realize scalable long distance qubit distribution telecommunication-wavelength photons and long-lived quantum memory elements are required [11]. Although multiplexing of atomic memory elements vastly improves the dependence of entanglement distribution on storage lifetime [12], there remains, the problem of robust atomic and photonic qubits for long-distance communication. Two-ensemble encoding suffers from the problem of long-term interferometric phase stability, while qubit states encoded in a single ensemble are hard to individually address.

A protocol for implementing entanglement distribution with an atomic ensemble-based quantum repeater has been proposed [5]. It involves generating and transmitting each of the qubit basis states individually, in practice via two interferometrically separate channels. Under prevailing conditions of low overall efficiencies it provides improved scaling compared to direct qubit entanglement distribution [4]. Its disadvantage is the necessity to stabilize the length of both transmission channels to a small

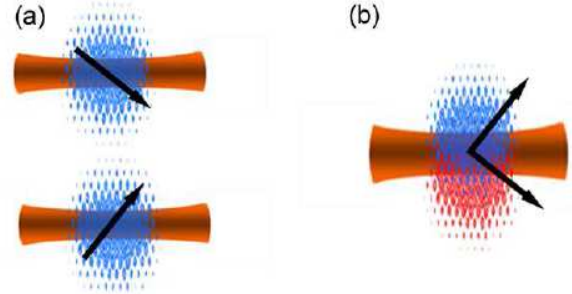


FIG. 1: (a) Schematic shows two orthogonal qubit states (arrows) encoded in two atomic ensembles coupled to distinct spatial light modes [5, 6], (b) the proposed architecture encodes the states in a two-species atomic mixture, coupled to a single light mode.

fraction of the optical wavelength, as the distribution of qubit entanglement is sensitive to the relative phase fluctuations in the two arms.

In this Letter we propose an interferometrically robust quantum repeater element based on entangled mixed-species atomic, and frequency-encoded photonic, qubits, Fig. 1. This avoids the use of two interferometrically separate paths for qubit entanglement distribution. The qubit basis states are encoded as single spin-wave excitations in each one of the two atomic species co-trapped in the same region of space. The spectroscopically resolved transitions enable individual addressing of the atomic species. Hence one may perform independent manipulations in the two repeater arms which share a single mode transmission channel. Phase stability is achieved by eliminating the relative ground state energy shifts of the co-trapped atomic species, as is in any case essential to successfully read out an atomic excitation [13].

We consider a co-trapped isotope mixture of ^{85}Rb and ^{87}Rb , containing, respectively, N_{85} and N_{87} atoms cooled in a magneto-optical trap, as shown in Fig. 2. Unpolarized atoms of isotope $(2f_{85}; 87g)$ are prepared in the ground hyperfine level $a^{()}$, where $a_E^{(85)}$

$$5S_{1=2}; F_a^{(85)} = 3, \quad a^{(87)} \quad 5S_{1=2}; F_a^{(87)} = 2, \quad \text{and}$$

$F_f^{()}$ is the total atomic angular momentum for level

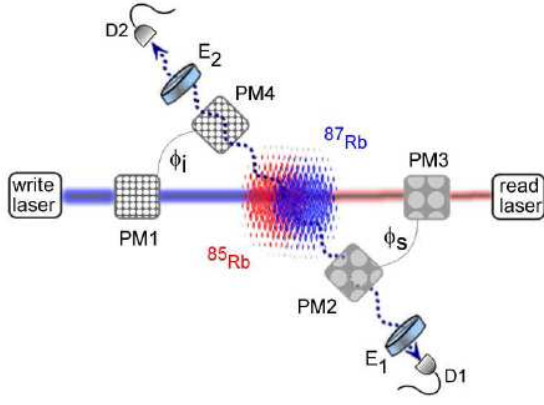


FIG. 2: Schematic of the experimental set-up showing the geometry of the addressing and scattered fields from the co-trapped isotope mixture of ^{85}Rb - ^{87}Rb . The write and read laser fields generate signal and idler fields, respectively detected at D1 and D2; E_1, E_2 are optical frequency filters. PM 1-4 are light phase modulators, ϕ_s and ϕ_i are relative phases of the driving rf fields, see text for details.

$f^{(i)}$. We consider the Raman configuration with ground levels $a^{(i)}$ and $b^{(i)}$ and excited level $c^{(i)}$ with energies $\sim |a^{(i)}|, \sim |b^{(i)}|$, and $\sim |c^{(i)}|$ respectively. Level $b^{(i)}$ corresponds to the ground hyperfine level with smaller angular momentum, while level $c^{(i)}$ is the $5P_{1=2}$ hyperfine level with $F_c^{(i)} = F_a^{(i)}$. A 150 ns long write laser pulse of wave vector $k_w = k_w \hat{y}$, horizontal polarization $e_{\text{R}} = \hat{z}$ and temporal profile $f(t)$ (normalized to unity $\int dt f(t)^2 = 1$) impinges on an electro-optic modulator (EOM), producing sidebands with frequencies $ck_w^{(85)} = ck_w + \omega_w$ and $ck_w^{(87)} = ck_w - \omega_w$ ($\omega_w = 531.5$ MHz) nearly resonant on the respective isotopic D_1 ($a^{(i)} \leftrightarrow c^{(i)}$) transitions with detunings $\Delta = ck_w^{(i)} - (|c^{(i)}| - |a^{(i)}|) \sim 10$ MHz. Spontaneous Raman scattering of the write fields results in signal photons with frequencies $ck_s^{(i)} = ck_w^{(i)} + (|b^{(i)}| - |a^{(i)}|)$ on the $b^{(i)} \leftrightarrow c^{(i)}$ transitions. The positive frequency component of the detected signal electric field from isotope i with vertical polarization e_v is given by

$$\hat{E}_1^{(i)(+)}(\mathbf{r}; t) = \frac{1}{2} \frac{ck_s^{(i)}}{\omega_0} e^{i ck_s^{(i)}(t - \hat{k}_s^{(i)} \cdot \mathbf{r})} u_s(\mathbf{r}) \hat{s}_s^{(i)}(t - \hat{k}_s^{(i)} \cdot \mathbf{r}) \phi, \quad (1)$$

where $u_s(\mathbf{r})$ is the transverse spatial profile of the signal field (normalized to unity in its transverse plane), and $\hat{s}_s^{(i)}(t)$ is the annihilation operator for the signal field. These operators obey the usual free field, narrow bandwidth bosonic commutation relations $[\hat{s}_s^{(i)}(t); \hat{s}_s^{(i)Y}(t^0)] = \delta(t - t^0)$. The emission of V -polarized signal photons creates correlated atomic spin-wave excitations with annihilation operators given by

$$\hat{s}^{(i)} = \cos \theta \hat{s}_1^{(i)} - \sin \theta \hat{s}_{+1}^{(i)}, \quad (2)$$

where

$$\cos^2 \theta = \frac{X_{m;1}^{(i)}}{X_{m;1}^{(i)2} + X_{m;0}^{(i)2}} = \frac{X_{m;1}^{(i)}}{X_{m;1}^{(i)2} + X_{m;0}^{(i)2}}; \quad (3)$$

$X_{m;1}^{(i)}$, $X_{m;0}^{(i)}$, $X_{m;-1}^{(i)}$ is a product of Clebsch-Gordan coefficients, and the spherical vector components of the spin wave are given by

$$\hat{s}_m^{(i)} = \frac{X_{m;1}^{(i)}}{P_{F_a^{(i)}} X_{m;1}^{(i)}} \hat{s}_{m;1}^{(i)}. \quad (3)$$

The spin wave Zeeman components of isotope i are given in terms of the i -th Rb atom transition operators $a^{(i)}_{jm}; b^{(i)}_{jm}$ and the write $u_w(\mathbf{r})$ and signal $u_s(\mathbf{r})$ field spatial profiles

$$\hat{s}_m^{(i)} = i A^{(i)} \frac{(2F_a^{(i)} + 1)^{1/2}}{N} e^{i(k_s^{(i)} - k_w^{(i)}) \cdot \mathbf{r}} u_s(\mathbf{r}) u_w(\mathbf{r}); \quad (4)$$

The effective overlap of the write beam and the detected signal mode [14] is given by

$$A^{(i)} = \frac{Z}{d^3} \int u_s(\mathbf{r}) u_w(\mathbf{r}) \int \frac{n^{(i)}(\mathbf{r})}{N} d^3 \mathbf{r}; \quad (5)$$

where $n^{(i)}(\mathbf{r})$ is the number density of isotope i . The interaction responsible for scattering into the collected signal mode is given by

$$\hat{H}_s(t) = i \omega_w f(t) \cos \theta \hat{s}_s^{(85)Y}(t) \hat{s}_s^{(85)Y} + \sin \theta \hat{s}_s^{(87)Y}(t) \hat{s}_s^{(87)Y} + \text{h.c.}; \quad (6)$$

where $P = \frac{2}{85} + \frac{2}{87}$ is a dimensionless interaction parameter,

$$P = \frac{2d_{cb}^{(i)} d_{ca}^{(i)} k_s^{(i)} k_w^{(i)} n_w^{(i)} N}{A^{(i)} (2F_a^{(i)} + 1) \sim 0} = \frac{V}{U} \frac{X_{m;1}^{(i)}}{X_{m;1}^{(i)2}}, \quad (7)$$

$d_{ca}^{(i)}$ and $d_{cb}^{(i)}$ are reduced matrix elements, $n_w^{(i)}$ is the average number of photons in the write pulse sideband with frequency $ck_w^{(i)}$, and the parametric mixing angle is given by $\cos^2 \theta = \frac{2}{85} = (\frac{2}{85} + \frac{2}{87})$. The interaction picture Hamiltonian also includes terms representing Rayleigh scattering and Raman scattering into undetected modes. One can show, however, that these terms commute with the signal Hamiltonian (Eq. (6)) and with the operators $\hat{s}_s^{(i)}(t)$ and $\hat{s}^{(i)}$ to order $O(1/N)$. As a result, the interaction picture density operator for the

signal-spin wave system (tracing over undetected idler modes) is given by $\hat{U} \hat{\rho}_0 \hat{U}^\dagger$, where $\hat{\rho}_0$ is the initial density matrix of the unpolarized ensemble and the vacuum electromagnetic field, and the unitary operator \hat{U} is given by

$$\ln \hat{U} = (\cos \hat{a}^{(85)y} \hat{s}^{(85)y} + \sin \hat{a}^{(87)y} \hat{s}^{(87)y} - i \hat{c}); \quad (8)$$

where $\hat{a}^{(\cdot)} = \int dt' (t) \hat{s}^{(\cdot)}(t)$ is the discrete signal mode bosonic operator. When the write pulse is sufficiently weak we may write $\hat{U} \approx 1 + (\cos \hat{a}^{(85)y} \hat{s}^{(85)y} + \sin \hat{a}^{(87)y} \hat{s}^{(87)y}) + O(\epsilon^2)$, i.e., the Raman scattering produces entanglement between a two-mode field (frequency qubit) and the isotopic spin wave (dual species matter qubit). Although we explicitly treat isotopically distinct species, it is clear that the analysis is easily generalized to chemically distinct atoms and/or molecules.

To characterize the nonclassical correlations of this system, the signal field is sent to an electro-optic phase modulator (PM 2 in Fig. 2) driven at a frequency $\omega_s = \omega_w + \omega_a^{(87)} - \omega_b^{(87)} + \omega_a^{(85)} - \omega_b^{(85)} = 2 = 1368$ MHz. The modulator combines the two signal frequency components into a central frequency $\omega_s = c(k_s^{(85)} + k_s^{(87)}) = 2$ with a relative phase ϕ_s . A photoelectric detector preceded by a filter (an optical cavity, E1 in Fig. 2) which reflects all but the central signal frequency is used to measure the statistics of the signal. We describe the detected signal field using the bosonic field operator,

$$\hat{s}^{(\cdot)}(t; s) = \frac{s^{(85)}}{2} e^{i\omega_s t} \hat{s}^{(85)}(t) + \frac{s^{(87)}}{2} e^{i\omega_s t} \hat{s}^{(87)}(t) + \frac{1}{2} e^{i\omega_s t} \hat{s}^{(85)}(t) + \frac{1}{2} e^{i\omega_s t} \hat{s}^{(87)}(t)$$

where $s^{(\cdot)} \in [0;1]$ is the signal efficiency including propagation losses and losses to other frequency sidebands within PM 2, and $\hat{s}^{(\cdot)}(t)$ represents concomitant vacuum noise. While quantum memory times in excess of 30 μ s have been demonstrated [15], here the spin wave qubit is retrieved after 150 ns by shining a vertically polarized read pulse into a third electro-optic phase modulator (PM 3 in Fig. 2), producing two sidebands with frequencies $\omega_r^{(85)}$ and $\omega_r^{(87)}$ resonant on the $b^{(85)} \rightarrow c^{(85)}$ and $b^{(87)} \rightarrow c^{(87)}$ transitions, respectively. This results in the transfer of the spin wave excitations to horizontally polarized idler photons emitted in the phase matched directions $k_i^{(\cdot)} = k_w^{(\cdot)} - k_s^{(\cdot)} + k_r^{(\cdot)}$. We treat the retrieval dynamics using the effective beam splitter relations $\hat{b}^{(\cdot)} = \sqrt{\eta_r^{(\cdot)}} \hat{s}^{(\cdot)} + \sqrt{1 - \eta_r^{(\cdot)}} \hat{r}^{(\cdot)}$, where $\eta_r^{(\cdot)}$ is the retrieval efficiency of the spin wave stored in the isotope Rb, $\hat{b}^{(\cdot)} = \int dt' (t) \hat{s}^{(\cdot)}(t)$ is the discrete idler bosonic operator for an idler photon of frequency $\omega_i^{(\cdot)}$, $\hat{r}^{(\cdot)}(t)$ is the temporal profile of an idler photon emitted from the Rb spin wave (normalized

to unity), and $\hat{r}_i^{(\cdot)}(t)$ is the annihilation operator for an idler photon emitted at time t . As with the signal operators, the idler field operators obey the usual free field, narrow bandwidth bosonic commutation relations $[\hat{r}_i^{(\cdot)}(t); \hat{r}_i^{(\cdot)\dagger}(t')] = \delta(t - t')$. A fourth EOM, PM 4, driven at a frequency $\omega_i = \omega_w + \omega_r^{(85)} - \omega_r^{(87)} = 2 = 531.5$ MHz combines the idler frequency components into a sideband with frequency $\omega_i = c(k_i^{(85)} + k_i^{(87)}) = 2$ with a relative phase ϕ_i . The combined idler field is measured by a photon counter preceded by a frequency filter (an optical cavity, E2 in Fig. 2) which only transmits fields of the central frequency ω_i . The detected idler field is described by the bosonic field operator,

$$\hat{r}_i^{(\cdot)}(t; i) = \frac{i^{(85)}}{2} e^{i\omega_i t} \hat{r}_i^{(85)}(t) + \frac{i^{(87)}}{2} e^{i\omega_i t} \hat{r}_i^{(87)}(t) + \frac{1}{2} e^{i\omega_i t} \hat{r}_i^{(85)}(t) + \frac{1}{2} e^{i\omega_i t} \hat{r}_i^{(87)}(t)$$

where $i^{(\cdot)} \in [0;1]$ is the idler efficiency including propagation losses and losses to other frequency sidebands within PM 4, and $\hat{r}_i^{(\cdot)}(t)$ represents associated vacuum noise. The write-read protocol in our experiment is repeated 2×10^6 times per second.

The signal-idler correlations result in phase-dependent coincidence rates given, up to detection efficiency factors, by $C_{si}(s; i) = \frac{1}{R} \frac{1}{R} \int dt_s \int dt_i \langle \hat{s}^\dagger(t_s; s) \hat{s}(t_s; s) \hat{r}_i^\dagger(t_i; i) \hat{r}_i(t_i; i) \hat{s}^\dagger(t_s; s) \rangle$.

From the state of the atom-signal system after the write process, $\hat{U} \hat{\rho}_0 \hat{U}^\dagger$, (Eq. 8), we calculate the coincidence rates to second order in ϵ ,

$$C_{si}(s; i) = \frac{2}{4} (s^{(85)})^2 \cos^2 \phi_s + (s^{(87)})^2 \sin^2 \phi_s + \frac{p}{(s^{(85)} s^{(87)})} \sin 2\phi_s \cos(\phi_i - \phi_s + \phi_0) \quad (9)$$

where $\phi_r^{(\cdot)}$, $\phi_i^{(\cdot)}$, $\phi_s^{(\cdot)}$, and ϕ_0 represent a real amplitude and phase, respectively, such that

$$e^{i\phi_0} = e^{i(\phi_s^{(85)} + \phi_i^{(85)})} \int dt' (t) \hat{r}_i^{(85)}(t) \hat{r}_i^{(87)}(t), \quad (10)$$

and we account for classical phase noise in the rf driving of the EOM pairs PM 1,4 and PM 2,3, by treating ϕ_s and ϕ_i as Gaussian random variables with variances σ_s^2 and σ_i^2 respectively, see Fig. 2. When the write fields are detuned such that the rates of correlated signal-idler coincidences are equal (i.e., when $(s^{(85)})^2 \cos^2 \phi_s = (s^{(87)})^2 \sin^2 \phi_s$), the fringe visibility is maximized, and Eq. (9) reduces to

$$C_{si}(s; i) = \frac{2}{2} (s^{(85)})^2 \cos^2 \phi_s [1 + \cos(\phi_i - \phi_s + \phi_0)]; \quad (11)$$

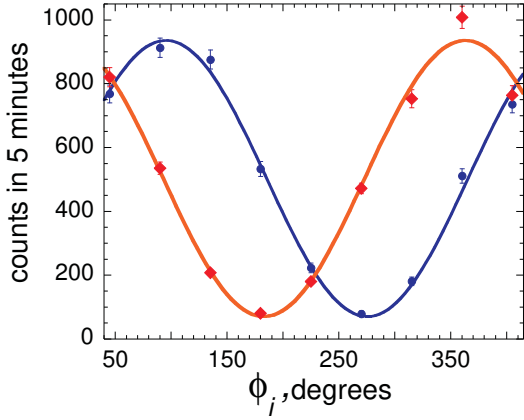


FIG. 3: Measured $C_{si}(s; i)$ as a function of i for $s = 0$, diamonds and for $s = -2$, circles. The angle ϕ_0 is absorbed into the arbitrary definition of the origin, i.e., ϕ_0 is deemed to be zero. Solid lines are sinusoidal fringes based on Eq. (11) with $V = 0.86$. Single channel counts of D1 and D2 show no dependence on the phases.

Fig. 3 shows coincidence fringes as a function of i taken for two different values of s . The detection rates measured separately for ^{85}Rb and ^{87}Rb were (a) 53 Hz and 62 Hz on D1 and (b) 95 Hz and 107 Hz on D2, respectively. These rates correspond to a level of random background counts about 2.5 times lower than the minima of the interference fringes. This implies that the observed value of visibility $V = 0.86$ cannot be accounted for by random photoelectric coincidences alone. The additional reduction of visibility may be due to variations in the idler phases caused by temporal variations in the cloud densities during data accumulation, while the effects of rf phase noise are believed to be negligible.

Following Ref. [16] we calculate the correlation function $E(s; i)$, given by

$$\frac{C_{si}(s; i) - C_{si}(s; i^?) - C_{si}(i^?; i) + C_{si}(i^?; i^?)}{C_{si}(s; i) + C_{si}(s; i^?) + C_{si}(i^?; i) + C_{si}(i^?; i^?)}, \quad (12)$$

where $i^?_{[i]} = s_{[i]} + i$. We note that, by analogy with polarization correlations, the detected signal [idler] field $\hat{a}_{s[i]}(t; i^?_{[i]})$ is orthogonal to $\hat{a}_{s[i]}(t; s_{[i]})$, i.e., $\langle \hat{a}_{s[i]}(t; s_{[i]}) | \hat{a}_{s[i]}^y(t^0; i^?_{[i]}) \rangle = 0$. One finds that a classical local hidden variable theory yields the Bell inequality $|S| \leq 2$, where $S = E(s; i) - E(s; i^?) - E(s; i^?) + E(s; i^?)$ [17]. Using Eq.(11), the correlation function is given by

$$E(s; i) = \cos(s - i + \phi_0). \quad (13)$$

Choosing, e.g., the angles $s = 0$, $i = -4$, $i^? = 0$, $i^? = 2$, and $i^? = 3 = -4$, we find the Bell parameter $S = 2.44$.

Table 1 presents measured values for the correlation function $E(s; i)$ using the canonical set of angles $s; i$. We find $S_{\text{exp}} = 2.44 \pm 0.04$ – a clear violation

TABLE I: Measured correlation function $E(s; i)$ and S for $t = 150$ ns delay between write and read pulses; all the errors are based on the statistics of the photon counting events.

s	i	$E(s; i)$
0	-4	0.629 ± 0.018
0	3 = -4	0.591 ± 0.018
-2	-4	0.614 ± 0.018
-2	3 = -4	0.608 ± 0.018
		$S_{\text{exp}} = 2.44 \pm 0.04$

of the Bell inequality. This value of S_{exp} is consistent with the visibility of the fringes $V = 0.86$ shown in Fig. 3. This agreement supports our observation that systematic phase drifts are negligible. We emphasize that no active phase stabilization of any optical frequency field is employed.

In conclusion, we report the first realization of a dual species matter qubit and its entanglement with a frequency-encoded photonic qubit. Although we employed two different isotopes, our scheme should work for chemically different atoms (e.g., rubidium and cesium) and/or molecules.

This work was supported by NSF, ONR, NASA, Alfred P. Sloan and Cullen-Peck Foundations. Present addresses: Dipartimento di Fisica e Matematica, Università dell'Insubria, 22100 Como, Italy; ²Laboratoire Aimé Cotton, CNRS-UPR 3321, Bâtiment 505, Campus Universitaire, 91405 Orsay Cedex, France; ³Department of Physics, University of Michigan, Ann Arbor, Michigan 48109.

-
- [1] C. H. Bennett et al, Phys. Rev. Lett. 70, 1895 (1993).
 - [2] A. K. Ekert, Phys. Rev. Lett. 67, 661 (1991).
 - [3] D. Bouwmeester et al, Nature (London) 390, 575 (1997).
 - [4] H. J. Briegel, W. Dür, J. I. Cirac, and P. Zoller, Phys. Rev. Lett. 81, 5932 (1998); W. Dür, H. J. Briegel, J. I. Cirac, and P. Zoller, Phys. Rev. A 59, 169 (1999).
 - [5] L.-M. Duan et al, Nature (London) 414, 413 (2001).
 - [6] D. N. Matsukevich and A. Kuzmich, Science 306, 663 (2004).
 - [7] D. N. Matsukevich et al, Phys. Rev. Lett. 95, 040405 (2005).
 - [8] D. N. Matsukevich et al, Phys. Rev. Lett. 96, 030405 (2006).
 - [9] C. W. Chou et al, Nature (London) 438, 828 (2005).
 - [10] H. de Riedmatten et al, Phys. Rev. Lett. 97, 113603 (2006).
 - [11] T. Chanelière et al, Phys. Rev. Lett. 96, 093604 (2006).
 - [12] O. A. Collins, S. D. Jenkins, A. Kuzmich, and T. A. B. Kennedy, quant-ph/0610036 (2006).
 - [13] D. N. Matsukevich et al, Phys. Rev. Lett. 96, 033601 (2006); S. D. Jenkins et al, Phys. Rev. A 73, 021803 (R) (2006).

- [14] S. D. Jenkins, Ph.D. Dissertation, Georgia Institute of Technology (2006).
- [15] D. N. Matsukevich et al., Phys. Rev. Lett. 97, 013601 (2006).
- [16] D. F. Walls and G. J. Milburn, Quantum Optics, (Springer-Verlag, 1994).
- [17] J. S. Bell, Physics 1, 105 (1964); J. S. Bell, Rev. Mod. Phys. 38, 447 (1966); J. F. Clauser, M. A. Home, A. Shimony, and R. A. Holt, Phys. Rev. Lett. 23, 880 (1969).